IRANIAN JOURNAL OF CATALYSIS

MgO support mediated enhancement of La_2BMnO_6 (B = Co, Ni) perovskite oxide in catalytic combustion of propane

Hamidreza Roozbahani[a], Sarah Maghsoodi[a*], Behrouz Raei[a], Amirhossein Shahbazi Kootenaei[a], and Zoha Azizi[a]

a) Department of Chemical Engineering, Mahshahr Branch, Islamic Azad University, Mahshahr, Iran.

Received 19 April 2023; received in revised form 29 June 2023; accepted 30 June 2023 (**DOI: 10.30495/IJC.2023.1984280.2004**)

ABSTRACT

Perovskite oxides possessing high stability and composition adjustability are effective in many applications. The La_2BMnO_6 (B=Co, Ni) double perovskite oxides were synthesized using the sol-gel method and deposited on MgO support (loading = 10, 20, and 30 wt. %) using a mechanical mixing method by an ultrasonic device. The elaborated samples were investigated for application in propane deep oxidation. The catalytic performance of these catalysts was analyzed by a variety of characterization techniques such as XRD, SEM, FTIR, TEM, and H_2-TPR. Ni-containing catalysts were found to have superior catalytic activity than the sample containing Co. The lowest catalytic activity belonged to the cobalt-containing double perovskite with 10 wt.% loading on MgO support, while the highest conversion was related to the $20La_2NiMnO_6$/MgO composite oxide with T_{90} = 434 °C. The support showed a positive impact on the performance of the catalysts. Deposition of a certain amount of perovskite oxides on the support boosted the specific surface area of the catalyst and, therefore, combined with improved reducibility, improved propane catalytic degradation.

***Keywords**: Double perovskite oxide; Support; Composite oxide; Catalytic combustion; Propane.*

1. Introduction

The most critical factors threatening human health seem to be environmental problems in the last century, exacerbated by air pollution. The major air pollutants are known as airborne particles, sulfur oxides, nitrogen oxides, and volatile organic compounds (VOCs). VOCs are considered an important class of air pollutants, which assume a broad group of compounds with different properties and chemistry while showing a similar behavior in the atmosphere. The detrimental effects of VOCs depend on their nature, concentration, and emission sources. These compounds can react with nitrogen oxide under the sunlight and, accordingly, cause stratospheric ozone destruction, climate change, plant rotting, and carcinogenic effects on humans [1-4]. Volatile organic compounds are organic chemicals with high vapor pressure at room temperature. The increasing release of VOCs into the environment is caused by urbanization and industrialization. The research on the elimination of volatile organic compounds has drawn the attention of many researchers in the last decades. Since the emission of VOCs, directly and indirectly, is seen as one of the main environmental pollutants, thus, minimizing the emission of VOCs seems highly essential. More than 50% of the released VOCs come from vehicles. Alkanes, including propane, are the major products of internal combustion engines. Catalytic oxidation is a promising technology for VOCs abatement. For, it provides high destructive efficiency at relatively lower temperatures [5-7].

Noble metal oxides are proper catalysts for combustion at low temperatures. However, the high cost and relatively limited thermal stability of these oxides trigger the research for alternative catalysts [8]. Meanwhile, perovskite oxide catalysts have demonstrated promising results for the oxidation of VOCs [5, 9]. Due to good activity and high thermal stability, single-perovskite catalysts seem to have a proper potential to replace noble metals in the removal

*Corresponding author:
E-mail address: maghsoodi_mahshahr@yahoo.com (**S. Maghsoodi**);

of the VOCs. Single perovskites can be generally described as ABO_3 or A_2BO_4 [10, 11]. In this general formula, A stands for the larger cation (A-site) with a 12-fold coordination, and B stands for the smaller cation (B-site) possessing a 6-fold coordination with the oxygen anions. Double perovskite oxides ($A_2B'B''O_6$) are produced by combining single perovskites [12]. The catalytic performance is enhanced in double perovskites as a result of further structural changes compared to single perovskites, and their activity may be equal to or higher than single perovskites in removing the VOCs [13, 14].

Perovskites have important advantages such as high flexibility in composition and structure, as well as resistance against poisoning with sulfur, phosphorus, and halogens, and high thermal stability. However, the biggest disadvantage of utilizing these materials is their low surface area and sintering at rather high temperatures [15-17].

Some studies have been conducted on enhancing the surface area of these materials, including changing the synthesis method and mounting perovskites on support. In this regard, forming a perovskite-support composite may be a practical and efficient method to prevent deactivation and increase mechanical strength.

Water pollution and the discharge of wastewater containing various organic and mineral pollutants into the water environment is considered as a critical challenge**.** In a recent study, $CaTiO_3$/g-C_3N_4 composite nanocatalyst was used to remove drug residues and photodegradation of GMF (Gemifloxacin) for photocatalytic wastewater treatment [18].

Due to its high melting point (2500 °C), MgO has high thermal stability. Thus, it can be used as catalyst support for high-temperature applications. Consequently, a proper combination of double perovskites and MgO may lead to the synthesis of a catalyst with not only the advantage of high-temperature stability but also excellent catalytic activity [19].

Despite the mentioned properties, few cases of double perovskites have been reported as combustion catalysts for propane oxidation. The relevant research has mostly focused on catalytic combustion and partial oxidation of methane. According to the literature, double perovskite oxides are highly active in methane combustion [20].

Pan et al. [21] investigated various single perovskites, including $LaCoO_3$, $LaMnO_3$, and $LaCuO_3$, and compared the performance with double perovskite catalysts such as La_2CoMnO_6 and La_2CuMnO_6. Experimental results revealed the better performance of double perovskites compared to single perovskites. Wang et al. [22] studied $La_{0.8}Ce_{0.2}MnO_3$ supported on CeO_2 for toluene deep oxidation. The obtained composite displayed higher catalytic performance due to high specific surface area, small grains, more oxygen vacancies, and highly reactive oxygen species.

Although much research has been done on the combustion activity of perovskites, the performance of supported perovskites has rarely been investigated. Here, we synthesized the support by a facile method and simply mounted the perovskite on the support demanding little equipment.

Herein, sol-gel elaborated double perovskites, La_2BMnO_6 (B=Co, Ni), were supported on a magnesium oxide support with various loadings. The physical and chemical properties of these materials were evaluated. The catalytic activity of the synthesized catalysts was measured at different reaction temperatures.

2. Experimental

2.1. Catalyst preparation

Double perovskite oxides of La_2BMnO_6 were used in this study, in which nickel (Ni) or cobalt (Co) transition metals are located in position B. The metal nitrate salts of the relevant elements were utilized to synthesize the perovskites. The double perovskite oxides were synthesized by the sol-gel method [23]. The support, MgO, was synthesized by the gel-combustion method from magnesium nitrate and examined as a catalyst support. The synthesized double perovskites were mounted on the support by ultrasonic mechanical mixing method with various loadings (wt.% = 10, 20, and 30). The materials used in the preparation of the catalysts are all purchased from Merck Company and used as received.

2.2. Sol-gel

First, distilled water (2 cc), citric acid (99.5%) (3.1 g), and ethylene glycol (>99%) (9.6 g) were mixed at 75 °C for 8 minutes. The molar ratio of citric acid to ethylene glycol was equal to 1. All calculations are based on preparing 1 gram of the catalysts considered. Then, manganese nitrate ($Mn(NO_3)_2.4H_2O$) (2.5 g) and cobalt nitrate ($Co(NO_3)_2.6H_2O$) (2.9 g) or nickel nitrate ($Ni(NO_3)_2.6H_2O$) (2.9 g) were added to obtain a clear and homogeneous solution. After that, lanthanum nitrate ($La(NO_3)_3.6H_2O$) (8.7 g) was added to the solution while the solution was under stirring and heated at 75 °C until it turned into a gel. This procedure was continued until the materials were fully dried. The molar

ratios of La, Mn, and M (M= Co or Ni) were considered to be 2:1:1. Ultimately, the obtained dried spongy material was pulverized. Finally, the calcination was carried out at 700 °C for 4 h in static air. The heating rate was 1 °C/min up to 300°C and 3°C/min up to 700 °C [24].

2.3. Gel-Combustion

The gel-combustion method was employed to prepare the MgO support. Calculated amounts of oxidizers and fuel (all purchased from Merck) were mixed with a small amount of distilled water in this method, which was heated at 75 °C to obtain a viscous paste. Magnesium nitrate ($Mg(NO_3)_2.6H_2O$) (6.4 g) and sorbitol ($C_6H_{14}O_6$) (1.7 g) were used as the oxidizer and as the fuel, respectively. The stoichiometric ratio of oxidizers to fuel was equal to 13:5. Afterward; the obtained paste was left to cool down for 15 min at ambient temperature. The resulting gel was transferred to a microwave (850 W) device for the combustion process. The achieved powder was then calcined in static air at 700 °C for 4 h [25].

2.4. Mechanical mixing

The mechanical mixing method was employed to mount the catalysts on the support. In this method, the synthesized double perovskite oxides with various loadings (wt. % = 10, 20, and 30) were mechanically mixed by an ultrasonic device with magnesium oxide and distilled water. The ultrasonic waves disperse particles in water. In the next stage, a filter paper was utilized to separate water from the sample. Then, the obtained materials were oven-dried at 110 °C overnight. After that, the dried sample was calcined in static air at 700 °C for 4 h. The obtained powder finally meshed in the range of 170~180 µm.

2.5. Catalyst characterization

The properties of all samples were determined using various techniques. The crystal structure of the catalysts was examined by X-ray diffraction analysis (XRD) using a PW1800 diffractometer (Philips Co.) (Cu-Kα, λ= 0.1541 nm). The diffraction intensity was measured for all samples in the range of $10°<2\theta<80°$ with a step size of 0.02˚ and 2 seconds for each step. The Debye-Scherrer equation was used to calculate the average size of the crystals:

$$d_{XRD} = \frac{k\lambda}{\beta \cos(\theta)} \quad (1)$$

Where d_{XRD}: The size of the crystals in nanometers, β: The width of the index peak in half of the peak height, and λ: The wavelength of the X-ray (0.15418 nm).

The specific surface area of the synthesized catalysts was determined using the BET technique. The samples were exposed to a stream of nitrogen with a flow rate of 20 cm^3/min before analysis, heated from the ambient temperature to 300 °C, and kept at this temperature for 2 h. The BET analysis was then performed by adsorption of nitrogen gas at -196 °C by the Nova Win2 device (manufactured by Quantachrome Company). The FTIR spectrum was measured using the KBr tablet technique by the PerkinElmer Spectrum apparatus. The morphological and structural properties of catalysts were specified using Scanning Electron Microscope (SEM) with a ZEISS device (EVO HD15 model) and Transmission Electron Microscope (TEM) with a ZEISS 10A device (Carl Zeiss-EM10C-100 KV model). The reducibility of the synthesized catalysts was probed by hydrogen temperature programmed reduction analysis (H_2-TPR) by the BELCAT A apparatus. The synthesized catalyst was heated under a stream of air from ambient temperature to 300 °C and kept at this temperature for one hour. The temperature of the sample was then reduced to the ambient temperature under the flow of the same gas. Afterward, the sample was exposed to a gas mixture flow of 7% hydrogen in argon up to a temperature of 900 °C. Ultimately, the amount of hydrogen consumed in the reduction process was calculated by integrating the areas under the TPR curves.

2.6. Catalyst activity evaluation

The catalytic combustion of propane was performed in a quartz fixed-bed reactor with a length of 80 cm and an internal diameter of 7 mm under atmospheric pressure. For each experiment, 0.1 g of the catalyst was mounted on quartz wool in the reactor. An electric furnace was employed for heating the reactor, and the catalyst was heated in dry air with a flow rate of 50 cm^3/min and a heating rate of 10 °C/min from ambient temperature to 500 °C. The reactor was then subjected to the flow of feed gas containing 4000 ppm propane in the air at a specific temperature. The reactor effluents were analyzed online by the Varian CP-3800 gas chromatography. The catalytic activity of perovskites at any temperature was calculated based on the propane conversion rate using the difference in concentrations at the inlet and outlet compared to the input concentration according to Eq. 2.

$$\text{Conversion (\%)}=\frac{[VOC]_{in}-[VOC]_{out}}{[VOC]_{in}}\times 100 \quad (2)$$

3. Results and Discussion

3.1. Catalyst characterization

3.1.1. Crystalline Phases (XRD) and specific surface area (BET)

The X-ray diffraction analysis was utilized to determine the crystalline phase of the elaborated samples. The double perovskite $A_2BB'O_6$ oxide can be described as a structure with B positions occupied by a combination of BO_6 and $B'O_6$ octahedra [13].

The XRD patterns are presented for the synthesized MgO as well as MgO-supported double perovskite oxide samples, La_2BMnO_6 (B= Co, Ni). **Fig. 1** shows the XRD spectra of MgO, La_2CoMnO_6, and $30La_2CoMnO_6$/MgO. According to the results, the diffraction peaks of the MgO sample (**Fig. 1a**) are mainly located at 37°, 43°, and 62°, which correspond to the standard X-ray diffraction patterns of magnesium oxide (JCPDS-43-1022) [26]. This confirms the presence of MgO in the investigated sample.

The XRD patterns of double perovskite oxide La_2CoMnO_6 synthesized by the sol-gel method are shown in **Fig. 1b**. It can be seen that diffraction peaks are consistent with the JCPDS-00-054-0834 card [27].

The X-ray diffraction patterns of double perovskite oxide La_2CoMnO_6 supported on MgO ($30La_2CoMnO_6$/MgO) are shown as a sample. The diffraction peaks are located at 2θ = 23°, 33°, 37°, 40°, 43°, 47°, 53°, 58°, 62°, and 68°. The obtained pattern demonstrates that the diffraction peaks of the examined catalyst are a combination of the diffraction peaks of the double perovskite and the support, which confirms the existence of a double perovskite structure besides magnesium oxide.

The XRD patterns of six supported catalysts are shown in **Fig. 2**. The diffraction peaks are almost similar for all the samples. All double perovskite oxide samples are completely combined with the support, and thereby, the interaction between the support and the perovskite phase is quite evident, with no observable impurity. Almost no crystalline phases other than MgO and La_2BMnO_6 were detected by the obtained XRD patterns in **Fig. 2**.

As can be realized from the acquired XRD patterns in **Fig. 2**, the main peak for all samples is located at 2θ=43°. In this work, the average crystal sizes of the supported catalysts were calculated using the Debye-Scherer equation (Eq. 1) [28, 29]. Accordingly, these sizes are within the range of 12~16 nm, as shown in **Table 1**. According to the previous literature, the crystal size of the double perovskite oxides has been reported to be more than 15 nm [23]. Thus, it is evident that MgO may be responsible for the lower crystal sizes of the dispersed perovskites at certain loadings. It has been suggested that a small amount of Mg^{2+} ions may be included in the double perovskite lattices since the ionic radius of Mg^{2+} is smaller than that of La^{3+} , but it has a larger radius than Mn^{3+} [30].

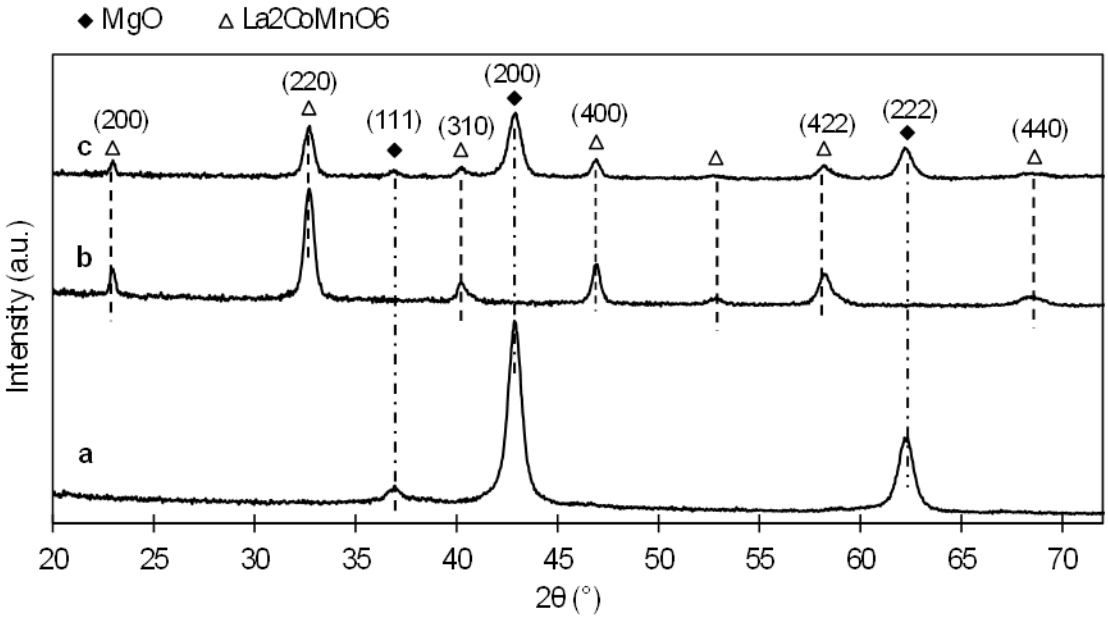

Fig. 1. X-ray diffraction pattern of (a) MgO, (b) La_2CoMnO_6 [22], and (c) $30La_2CoMnO_6$/MgO calcined in static air at 700 °C for 4 h.

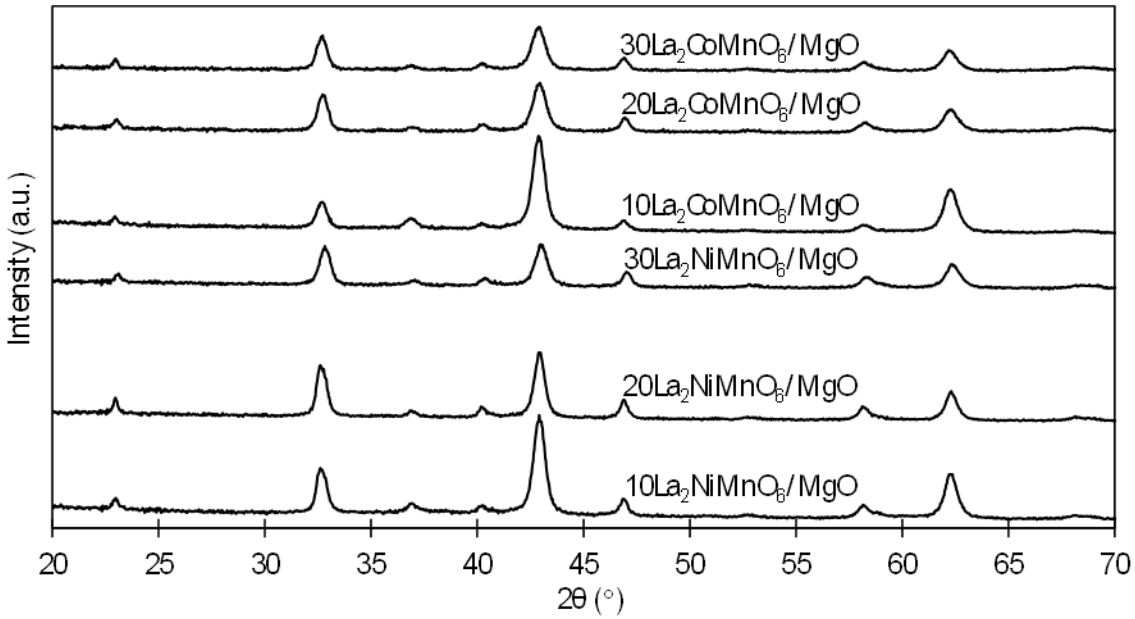

Fig. 2. XRD patterns of La_2BMnO_6/MgO (B= Co, Ni) with various loadings (10, 20, and 30 wt.%) calcined in static air at 700 °C for 4 h.

Table 1: Crystal size and S_{BET} of MgO, La_2BMnO_6 [22], La_2BMnO_6/MgO (B= Co, Ni) with various loadings (10, 20, and 30 wt.%) calcined in static air at 700 °C for 4 h.

Sample	Crystal size [nm]	S_{BET} [m^2g^{-1}]
MgO	11	55
La_2NiMnO_6	19	22
$10La_2NiMnO_6$/MgO	16	59
$20La_2NiMnO_6$/MgO	14	75
$30La_2NiMnO_6$/MgO	14	61
La_2CoMnO_6	15	23
$10La_2CoMnO_6$/MgO	13	56
$20La_2CoMnO_6$/MgO	12	70
$30La_2CoMnO_6$/MgO	12	60

The measured BET-specific surface areas of the catalysts (S_{BET}) are presented in **Table 1**. The $20La_2NiMnO_6$/MgO catalyst possesses the largest specific surface area (75 m^2g^{-1}). According to previous studies [13], increasing the specific surface area might be responsible for the enhancement of the catalytic performance of the investigated catalysts.

From **Table 1**, it can be concluded that for equal perovskite loading, Ni-containing catalysts have a larger specific surface area than Co-containing catalysts. The $10La_2CoMnO_6$/MgO sample has the lowest specific surface being equal to 56 m^2g^{-1}.

Evaluating the specific surface areas of pure double perovskite oxides in previous articles and comparing them with the results in **Table 1** leads us to claim that the presence of the support has enhanced the specific surface areas of the catalysts. Thus, the presence of support can increase the specific surface areas of catalysts and improve the effective dispersion of active sites [13, 31]. The dispersion of double perovskite oxides on the support has been improved for catalysts with 20 wt.% perovskite loading. However, increasing the loading of double perovskites to 30 wt.% led to a specific surface area decline, which can be attributed to the penetration of double perovskites into the MgO lattices and the contraction of the perovskite network by Mg^{2+} ions.

3.1.2. FTIR study

The infrared spectra of the supported double perovskite oxide samples are presented in **Fig. 3**. The IR spectra of all samples presented typical patterns, indicating the presence of two strong and defined bands. These patterns are similar to the structure of other $A_2BB'O_6$ and represent the characteristic of the structure of perovskites [32]. The vibrational bands appear between 400 cm^{-1} and 900 cm^{-1} and originate from the stretching property of the Mg-O bond [33]. This vibration band is found between 400 cm^{-1} and 600 cm^{-1} in the case of the double perovskites, which is known as the result of the stretching and bending vibrations of the B-O bond in the BO_6 octahedron [13]. The BO_6 octahedral moieties usually have a stronger bond in the double perovskites structure, and their vibrational behavior is related to the characteristics of stretching and asymmetric states of bonds due to the presence of two metal cations in the octahedral sites of the unit cell.

The obtained patterns indicate that the intensities of double perovskites bands are stronger than that of MgO. As can be realized, the new absorption bands have occurred between 400 cm^{-1} and 700 cm^{-1} after mounting double perovskites on the support, and the energy intensity of the bands shifts towards the higher wavelength. Moreover, according to **Fig. 3**, the lower the weight percentage of the support, the stronger the intensity of the bands would be.

The spectroscopic data on the infrared frequencies of the catalysts (**Table 2**) suggests that in the supported samples stretching vibrations between Ni-O, Co-O, and Mn-O occurred in the high energy region in ~700 cm^{-1} band (V2), and thereby, the Mn^{4+}-O bond has become somewhat stronger than other bonds [32]. The Ni-O and Co-O bands overlap with a weaker intensity than the Mn-O band. Therefore, M^{2+} ions seem to affect the M-O-Mn linking units [32]. Hence, this strong absorption occurs due to the asymmetric stretching of the MnO_6 polyhedron. On the other hand, the low-energy region (V1) of ~410 cm^{-1} can be attributed to the La-O stretching state, which in turn indicates the formation of the double perovskite [34].

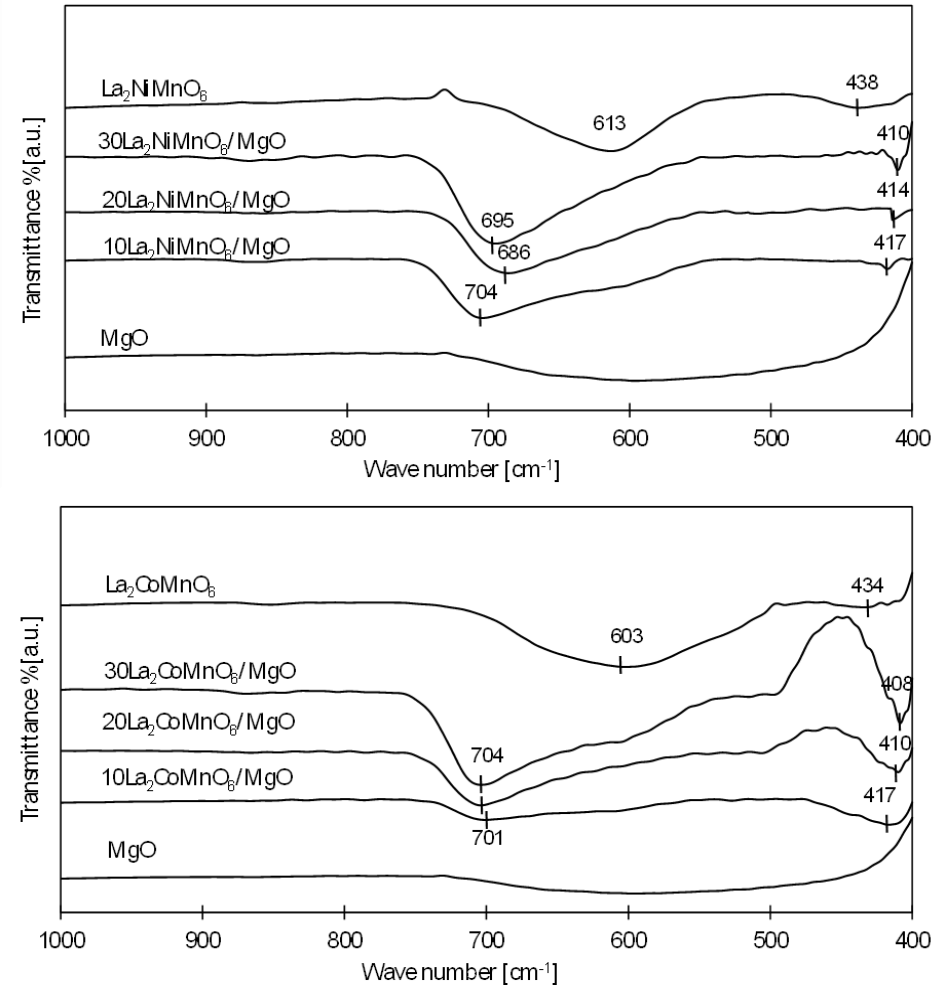

Fig. 3: FTIR spectra of MgO, La_2BMnO_6 [22], and La_2BMnO_6/MgO (B= Co, Ni) with various loadings (10, 20, and 30 wt.%) calcined in static air at 700 °C for 4 h.

Table 2: FTIR spectroscopic data of La_2BMnO_6 [22], La_2BMnO_6/MgO (B= Co, Ni) with various loadings (10, 20, and 30 wt.%) calcined in static air at 700 °C for 4 h.

Oxides	Infrared frequencies [cm^{-1}]	
	ν_2	ν_1
La_2NiMnO_6	613	438
$10La_2NiMnO_6$/MgO	704	417
$20La_2NiMnO_6$/MgO	686	414
$30La_2NiMnO_6$/MgO	695	410
La_2CoMnO_6	603	434
$10La_2CoMnO_6$/MgO	701	417
$20La_2CoMnO_6$/MgO	704	410
$30La_2CoMnO_6$/MgO	704	408

As evidenced by the acquired FTIR spectra, band shift is discernable for the supported double perovskites. This can be explained by the interaction between the perovskite phase and MgO support. This observation is reported by other groups [35].

3.1.3. Morphology study

The SEM images were utilized to characterize the morphology of the supported catalysts. The SEM image of $20La_2NiMnO_6$/MgO is presented in **Fig. 4**. It can be seen that the sample exhibits spongy morphology. This is suggested to be a consequence of the production of large amounts of gas during the preparation of the support, which has led to the formation of MgO with spongy morphology, and this, in turn has increased the volume of the pores [25]. Accordingly, the increased surface area of the support may be responsible for the higher S_{BET} of the supported catalysts [36]. It is suggested that high porosity can enhance the catalyst activity due to increasing the contact surfaces of the reactant with the catalyst. The presented SEM image of the $20La_2NiMnO_6$/MgO composite oxide reveals that the sample possesses relatively good uniformity, and no aggregation of the catalyst particles can be observed.

The TEM micrograph was used to observe more details of the synthesized particles (**Fig. 5**). It is observable that larger particles are made up of much smaller particles, and these small particles are indeed composed of other non-spherical nanoparticles.

As can be seen in **Fig. 5**, utilizing MgO as a support has successfully led to a good dispersion of La_2NiMnO_6 particles on the support surface. The problem of sintering is known as one of the factors reducing the catalytic activity of double perovskites. In the case of supported samples, MgO effectively lessened the sintering of the La_2MnNiO_6 particles.

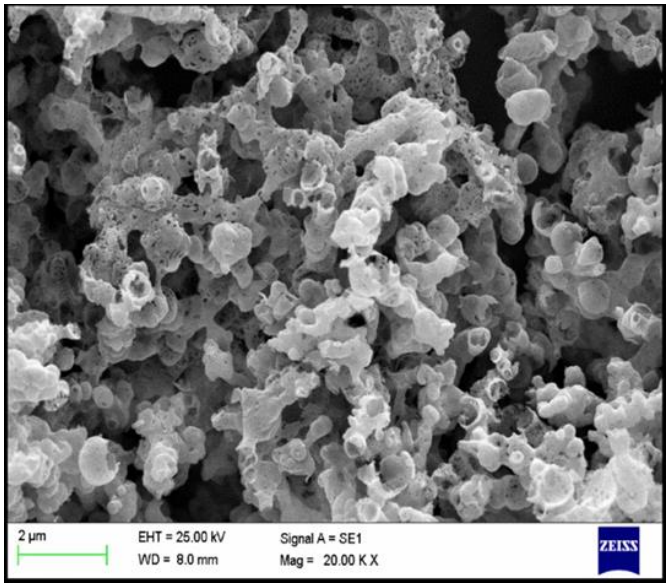

Fig. 4: SEM micrograph of $20La_2NiMnO_6$/MgO calcined in static air at 700 °C for 4 h.

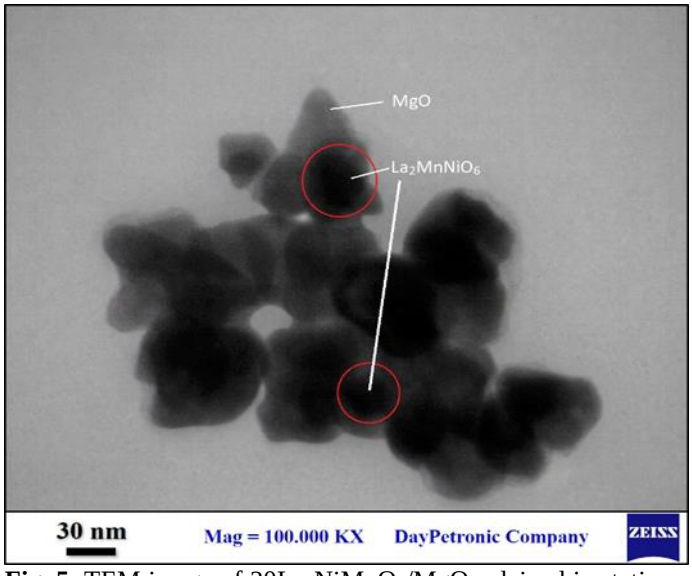

Fig. 5: TEM image of $20La_2NiMnO_6$/MgO calcined in static air at 700 °C for 4 h.

3.1.4. H_2-TPR study

The H_2-TPR technique was utilized to evaluate the reactivity of oxygen species and the impact of the support on the reducibility of the double perovskite oxides. The H_2-TPR technique reduces high-valence metal ions and oxygen species (surface and intra-lattice) [37]. The H_2-TPR profiles for the synthesized catalysts with different perovskite loadings are presented in **Fig. 6**.

Two reduction peaks are discernible from the graphs obtained for the nickel-containing catalysts (La_2NiMnO_6/MgO), representing two stages of reduction. In the first stage of the reduction, oxygen species on the surface of the catalysts are reduced at lower temperatures. In the meanwhile, Mn^{4+} and Ni^{3+} ions are reduced to Mn^{3+} and Ni^{2+} ions, respectively [38]. This phenomenon may happen due to a decrease in the amount of reducible oxygen in the bulk perovskite or a decrease in the lattice oxygen migration from the inside toward the surface. The second stage of reduction, at higher temperatures, is related to the reduction of oxygen species in the bulk perovskite lattice [39]. In the second peak, the Ni^{2+} ion is reduced to Ni^0 [38].

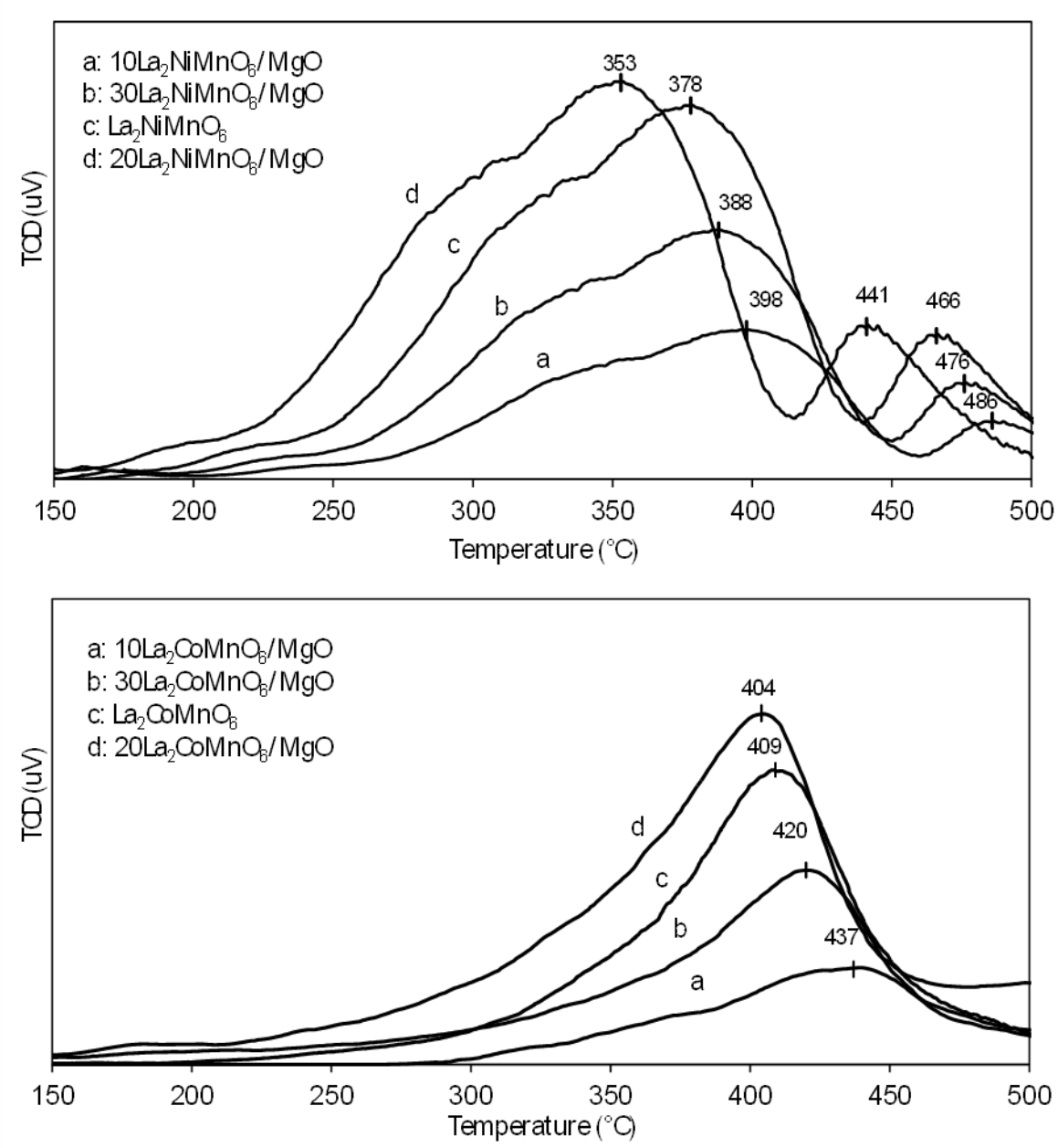

Fig. 6: H_2-TPR profiles of the catalysts La_2BMnO_6 [22] and La_2BMnO_6/MgO (B= Co, Ni) with various loadings (10, 20, and 30 wt.%) calcined in static air at 700 °C for 4 h.

The H_2-TPR profiles of the cobalt-containing catalysts represent a reduction stage between 250 °C and 500 °C, which occurs due to the reduction of Mn^{4+} to Mn^{3+} and Co^{3+} to Co^{2+}. The mentioned peaks of Mn and Co seem to have some overlapping [21].

The reduction of La^{3+} basically demands rather high temperatures in the H_2-TPR process. Therefore, the peaks of H_2 consumption in the TPR diagrams can be mainly attributed to the reduction of site B metals and MgO [31]. Thermodynamically, manganese cations' oxidation and metallic manganese formation are not feasible [40]. Meanwhile, Mg^{2+} ions cannot be reduced in the studied temperature range since these ions seem to be highly stable in the structure of MgO [39].

The area of the H_2-TPR curves represents the amount of hydrogen consumed during the reduction process. The peak area and peaks temperatures are known to be possible factors in the reduction process that may be in accordance with the activity of the catalyst. It is suggested that a larger peak area and a lower temperature of the peak are related to the better reducibility of the catalysts [19].

The temperature of the peak of the Ni-containing samples is the lowest among other investigated samples. Also, the area under the curve is larger (**Table 3**). Thus, they may possess higher reducibility. This suggests that the presence of nickel and its interaction with manganese significantly facilitates the reduction of the catalyst. It is also observed that perovskite loading on the support can influence the amount of hydrogen consumption.

Table 3 shows the total amount of the consumed H_2. One can realize that the higher activity of the catalyst is synchronized with higher hydrogen consumption. On the other hand, the amount of hydrogen consumption of certain loadings of supported Ni-containing double perovskites is higher than that of Co-containing double perovskites. According to the data obtained, the $20La_2NiMnO_6/MgO$ sample possesses the highest hydrogen consumption, which accordingly has the highest combustion activity.

In comparison with the previous literature [19], one may understand from the presented graphs and tables related to the TPR profile that the presence of support has increased the reduction temperature except for MgO supported $20La_2BMnO6$ (B= Co, Ni). This can be attributed to the partial substitution of Mg^{2+} in the structure of double perovskites and the interaction between the support and the catalyst.

3.2. Catalytic combustion of propane

The effect of MgO support on the catalytic performance of double perovskites La_2BMnO_6 (B= Co, Ni) synthesized by the sol-gel method was evaluated for propane oxidation in the temperature range of 100 °C to 500 °C. The reaction conversion at each temperature was measured as shown in **Fig. 7**. All the samples displayed an S-shaped profile (**Fig. 7a**) for propane conversion as a function of the reaction temperature under identical experimental conditions. In general, the catalytic performance of double perovskite oxides amplifies as the temperature rises. As can be seen in **Fig. 7a**, the propane conversion is less than 10% at temperatures below 200 °C, which can be confirmed by the TPR profiles.

According to the literature, one can claim that molecular oxygen, after being adsorbed on the perovskite surface, generates dissociated oxygen species, which in turn can be incorporated into the crystal lattice of perovskite. These species can react with adsorbed methane

Table 3: Results of H_2-TPR of La_2BMnO_6 [22], La_2BMnO_6/MgO (B= Co, Ni) with various loadings (10, 20, and 30 wt.%) calcined in static air at 700 °C for 4 h.

Catalyst	H_2 Uptake (μmol H_2/g of catalyst)
La_2NiMnO_6	1032
$10La_2NiMnO_6/MgO$	476
$20La_2NiMnO_6/MgO$	1291
$30La_2NiMnO_6/MgO$	762
La_2CoMnO_6	1028
$10La_2CoMnO_6/MgO$	276
$20La_2CoMnO_6/MgO$	1141
$30La_2CoMnO_6/MgO$	332

according to the Mars-Van-Krevelen mechanism. During the reaction, reduction of the metal oxide occurs. The reduced metal oxide is oxidized again by the gas phase oxygen present in the feed [13, 25]. The first-order reaction equation was used to evaluate the kinetic parameters with the formula $\ln[-\ln(1-X)]=\ln A-E_a/RT$. In this equation, apparent activation energy (E_a) and the exponential factor (A) can be evaluated by a correlation utilizing propane conversion, X, and reaction temperature, T [31].

The function ln[-ln(1-X)] was drawn vs. 1000/T as shown in **Fig. 7b**. Then, the apparent activation energy was calculated using the slope of the straight line, which is shown in **Table 4**.

Table 4: Temperatures at 10% (T_{10}), 50% (T_{50}), and 90% (T_{90}) conversion of propane, and activation energies over the La_2BMnO_6/MgO (B = Ni and Co with various loadings (10, 20, and 30 wt.%) calcined in static air at 700 °C for 4 h.

Sample	Catalytic Activity (°C)			Activation Energy (kJ/mol)
	T_{10}	T_{50}	T_{90}	
$10La_2NiMnO_6/MgO$	328	430	490	78
$20La_2NiMnO_6/MgO$	276	367	434	54
$30La_2NiMnO_6/MgO$	325	412	486	77
$10La_2CoMnO_6/MgO$	331	434	495	79
$20La_2CoMnO_6/MgO$	290	374	440	56
$30La_2CoMnO_6/MgO$	330	432	493	79

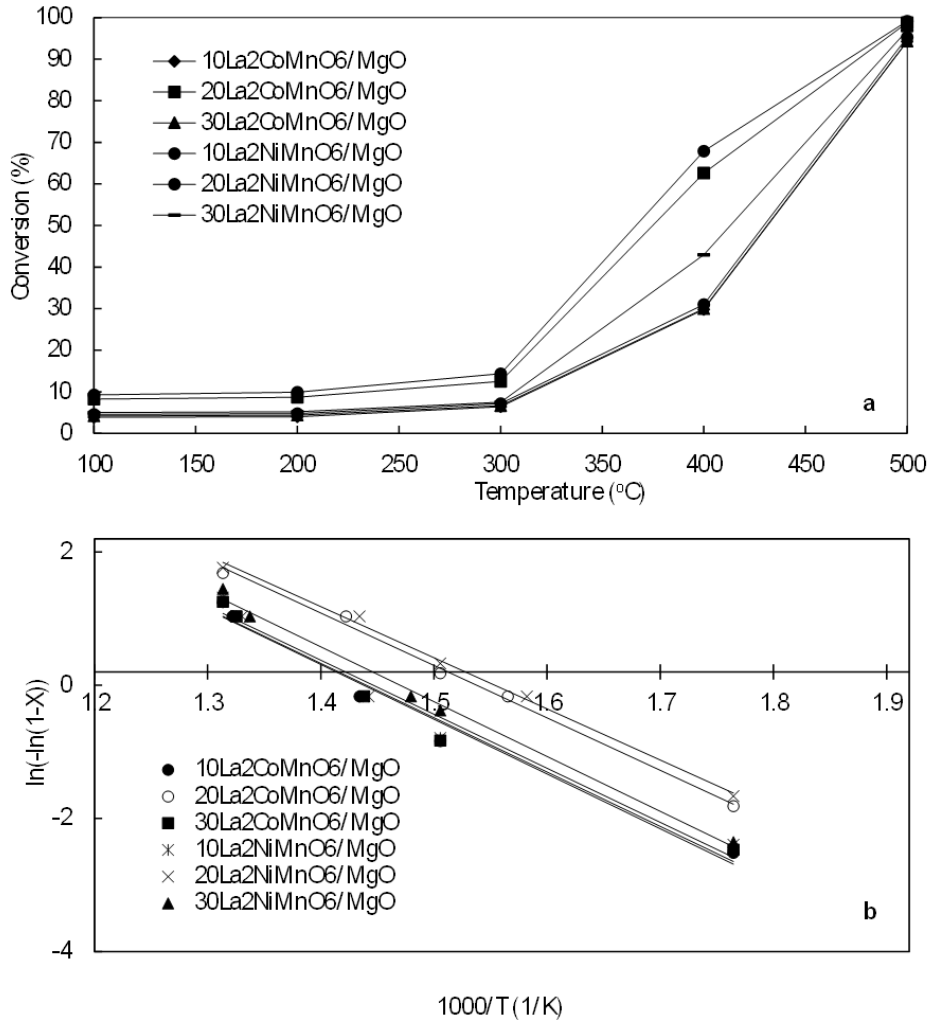

Fig. 7: (a) Catalytic activities of the catalysts in the combustion of propane, and (b) Arrhenius plots of reaction rates over La_2BMnO_6/MgO (B= Co, Ni) with various loadings (10, 20, and 30 wt.%) calcined in static air at 700 °C for 4 h.

According to previous studies, propane catalytic combustion reaction kinetics is a first-order kinetic model under steady-state assumption [41]. The activation energy of propane combustion catalysts has been reported in the range of 50~100 (kJ/mol) in the previous literature, suggesting that the evaluated activation energies in this study are comparable to the results obtained by other groups [41, 42].

The activity of the catalysts was reported using T_{10}, T_{50}, and T_{90} values as the temperature needed for converting 10%, 50%, and 90% of propane, respectively, in **Table 4**. The composite oxide $20La_2NiMnO_6/MgO$ demonstrated that its 10%, 50%, and 90% conversion temperatures are lower compared to other catalysts. One can realize from the activation energy values in **Table 4** that nickel-containing double perovskites have a lower activation energy than cobalt-containing double perovskites.

According to the BET results, the highest specific surface area and crystal size belong to the $20La_2NiMnO_6/MgO$ sample, and this can be a reason for the better performance of the catalyst, although no direct relationship was found between activity and crystallinity.

The nickel-containing samples had a higher conversion than cobalt-containing samples (except for the $20La_2NiMnO_6/MgO$ catalyst), so the nature of B-site cations can be a determining factor in catalytic activity. By increasing the amount of catalyst up to 20%, the catalyst conversion has also increased, reaching maximum performance. Higher loadings (30 wt.%) led to a reduction in the activity of the catalysts, which can be attributed to the decrease in active surfaces, the reduction of active cations reducibility, and the decreased interactions between the catalyst and the support.

4. Conclusions

The double perovskite-MgO composites synthesized by the ultrasonic method were investigated in this research. The XRD analysis results demonstrated that the perovskite structure of all the synthesized catalysts has been formed, and the perovskite phase was the only discernible crystalline phase. It was found that the composite oxides $20La_2NiMnO_6/MgO$ possessed superior catalytic performance among the probed samples for propane combustion due to more specific surface area and better reducibility. The presence of the support led to the augmentation of the activity of the catalysts. Samples with 20 wt.% loading showed the best performance. By increasing the loading of double perovskites to 30 wt.%, the performance of the catalysts decreased. The highest and lowest conversion were recorded for the $20La_2NiMnO_6/MgO$ and $10La_2CoMnO_6/MgO$ composite oxides, respectively.

Acknowledgements

We thank the Mahshahr Branch, Islamic Azad University, for the financial support.

References

[1] M.S. Kamal, S.A. Razzak, M.M. Hossain, Atmos. Environ. 140 (2016) 117-134.

[2] M. Tomatis, H.-H. Xu, J. He, X.-D. Zhang, J. Chem. 2016 (2016) 8324826.

[3] Z. Zhang, Z. Jiang, W. Shangguan, Catal. Today. 264 (2016) 270-278.

[4] C. He, J. Cheng, X. Zhang, M. Douthwaite, S. Pattisson, Z. Hao, Chem. Rev. 119 (2019) 4471-4568.

[5] M. Zang, C. Zhao, Y. Wang, S. Chen, J. Saudi Chem. Soc. 23 (2019) 645-654.

[6] Y. Guo, M. Wen, G. Li, T. An, Appl. Catal. B Environ. 281 (2021) 119447.

[7] R. Liu, H. Wu, J. Shi, X. Xu, D. Zhao, Y.H. Ng, M. Zhang, S. Liu, H. Ding, Catal Sci Technol. 12 (2022) 6945-6991.

[8] L.F. Liotta, Appl. Catal. B Environ. 100 (2010) 403-412.

[9] H. Li, J. Yu, Y. Gong, N. Lin, Q. Yang, X. Zhang, Y. Wang, Sep. Purif. Technol. 307 (2023) 122716.

[10] A. Zhao, Y. Ren, H. Wang, Z. Qu, J. Environ. Sci. 127 (2023) 811-823.

[11] J. Cho, M. Kim, I. Yang, K.T. Park, C.H. Rhee, H.W. Park, J.C. Jung, J. Rare Earths. (2023)

[12] S. Vasala, M. Karppinen, Prog. Solid State Chem. 43 (2015) 1-36.

[13] J.E. Tasca, A.E. Lavat, M.G. González, J. Asian Ceram. Soc. 5 (2017) 235-241.

[14] X. Gao, Z. Jin, R. Hu, J.n. Hu, Y. Bai, P. Wang, J. Zhang, C. Zhao, J. Rare Earths. 39 (2021) 398-408.

[15] M. Wu, H. Li, S. Ma, S. Chen, W. Xiang, Sci. Total Environ. 795 (2021) 148904.

[16] J. Yang, S. Hu, L. Shi, S. Hoang, W. Yang, Y. Fang, Z. Liang, C. Pan, Y. Zhu, L. Li, J. Wu, J. Hu, Y. Guo, Environ. Sci. Technol. 55 (2021) 9243-9254.

[17] C. Feng, Q. Gao, G. Xiong, Y. Chen, Y. Pan, Z. Fei, Y. Li, Y. Lu, C. Liu, Y. Liu, Appl. Catal. B Environ. 304 (2022) 121005.

[18] M. Foroughipour, A. Nezamzadeh-Ejhieh, Chemosphere 334 (2023) 139019.

[19] E.E. Svensson, S. Nassos, M. Boutonnet, S.G. Järås, Catal. Today. 117 (2006) 484-490.

[20] R. Hu, R. Ding, J. Chen, J. Hu, Y. Zhang, Catal. Commun. 21 (2012) 38-41.

[21] K.L. Pan, G.T. Pan, S. Chong, M.B. Chang, J. Environ. Sci. 69 (2018) 205-216.

[22] Y. Wang, Y. Xue, C. Zhao, D. Zhao, F. Liu, K. Wang, D.D. Dionysiou, J. Chem. Eng. 300 (2016) 300-305.

[23] H. Roozbahani, S. Maghsoodi, B. Raei, A.S. Kootenaei, Z. Azizi, Korean J. Chem. Eng. 39 (2022) 586-595.

[24] A. Jahangiri, H. Pahlavanzadeh, H. Aghabozorg, Int. J. Hydrog. Energy, 37 (2012), 9977-9984.

[25] S. Maghsoodi, J. Towfighi, A. Khodadadi, Y. Mortazavi, J. Chem. Eng. 215-216 (2013) 827-837.

[26] K.R. Nemade, S.A. Waghuley, Int. J. Met. 2014 (2014) 389416.

[27] J. Fu, H.-y. Zhao, J.-r. Wang, Y. Shen, M. Liu, Int. J. Miner. Metall. 25 (2018) 950-956.

[28] SD Khairnar, MR Patil, VS Shrivastava, Iranian Journal of Catalysis 8(2), (2018), 143-150.

[29] A Yousefi, A Nezamzadeh-Ejhieh, Iran. J. Catal. 11(3), (2021), 247-259.

[30] R. Shaheen, J. Bashir, Solid State Sci. 12 (2010) 1496-1499.

[31] J. Li, R. Hu, J. Zhang, W. Meng, Y. Du, Y. Si, Z. Zhang, Fuel. 178 (2016) 148-154.

[32] A.E. Lavat, E.J. Baran, Vib Spectrosc. 32 (2003) 167-174.

[33] S. Li, Int. J. Ind. Chem. 10 (2019) 89-96.

[34] C. Li, B. Liu, Y. He, C. Lv, H. He, Y. Xu, J. Alloys Compd. 590 (2014) 541-545.

[35] A. Norouzi, A. Nezamzadeh-Ejhieh, Physica B 599, (2020), 412422.

[36] P. Kumar Yadav, T. Das, P. Mondal, Fuel. 302 (2021) 121233.

[37] K. Bakhtiari, A. Shahbazi Kootenaei, S. Maghsoodi, S. Azizi, S.M. Tabatabaei Ghomsheh, Ceram. Int. 48 (2022) 37394-37402.

[38] S. Cimino, L. Lisi, R. Pirone, G. Russo, M. Turco, Catal. Today. 59 (2000) 19-31.

[39] R. Ding, C. Li, L. Wang, R. Hu, Appl. Catal. A Gen. 464-465 (2013) 261-268.

[40] F. Touahra, A. Rabahi, R. Chebout, A. Boudjemaa, D. Lerari, M. Sehailia, D. Halliche, K. Bachari, Int. J. Hydrog. Energy. 41 (2016) 2477-2486.

[41] G. Chai, W. Zhang, L.F. Liotta, M. Li, Y. Guo, A. Giroir-Fendler, Appl. Catal. B Environ. 298 (2021) 120606.

[42] Z. Liu, L. Cheng, J. Zeng, X. Hu, S. Zhangxue, S. Yuan, Q. Bo, B. Zhang, Y. Jiang, J. Solid State Chem. 292 (2020) 121712.